NASA/TM-2000-210121

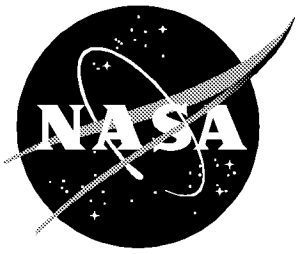

Flow Visualization by Elastic Light Scattering in the Boundary Layer of a Supersonic Flow

G. C. Herring and Mervin E. Hillard, Jr.
Langley Research Center, Hampton, Virginia

August 2000

The NASA STI Program Office . . . in Profile

Since its founding, NASA has been dedicated to the advancement of aeronautics and space science. The NASA Scientific and Technical Information (STI) Program Office plays a key part in helping NASA maintain this important role.

The NASA STI Program Office is operated by Langley Research Center, the lead center for NASA's scientific and technical information. The NASA STI Program Office provides access to the NASA STI Database, the largest collection of aeronautical and space science STI in the world. The Program Office is also NASA's institutional mechanism for disseminating the results of its research and development activities. These results are published by NASA in the NASA STI Report Series, which includes the following report types:

- TECHNICAL PUBLICATION. Reports of completed research or a major significant phase of research that present the results of NASA programs and include extensive data or theoretical analysis. Includes compilations of significant scientific and technical data and information deemed to be of continuing reference value. NASA counterpart of peer-reviewed formal professional papers, but having less stringent limitations on manuscript length and extent of graphic presentations.

- TECHNICAL MEMORANDUM. Scientific and technical findings that are preliminary or of specialized interest, e.g., quick release reports, working papers, and bibliographies that contain minimal annotation. Does not contain extensive analysis.

- CONTRACTOR REPORT. Scientific and technical findings by NASA-sponsored contractors and grantees.

- CONFERENCE PUBLICATION. Collected papers from scientific and technical conferences, symposia, seminars, or other meetings sponsored or co-sponsored by NASA.

- SPECIAL PUBLICATION. Scientific, technical, or historical information from NASA programs, projects, and missions, often concerned with subjects having substantial public interest.

- TECHNICAL TRANSLATION. English-language translations of foreign scientific and technical material pertinent to NASA's mission.

Specialized services that complement the STI Program Office's diverse offerings include creating custom thesauri, building customized databases, organizing and publishing research results . . . even providing videos.

For more information about the NASA STI Program Office, see the following:

- Access the NASA STI Program Home Page at ***http://www.sti.nasa.gov***

- Email your question via the Internet to help@sti.nasa.gov

- Fax your question to the NASA STI Help Desk at (301) 621-0134

- Telephone the NASA STI Help Desk at (301) 621-0390

- Write to:
  NASA STI Help Desk
  NASA Center for AeroSpace Information
  7121 Standard Drive
  Hanover, MD 21076-1320

NASA/TM-2000-210121

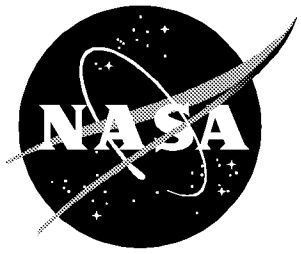

Flow Visualization by Elastic Light Scattering in the Boundary Layer of a Supersonic Flow

G. C. Herring and Mervin E. Hillard, Jr.
Langley Research Center, Hampton, Virginia

National Aeronautics and
Space Administration

Langley Research Center
Hampton, Virginia 23681-2199

August 2000

Acknowledgments

We are pleased to thank R. W. Gregory and W. E. Lipford for help with the optical setup, K. Stacy for image processing and video production, J. Thibodeaux for overseeing the model preparation, and the UPWT operations staff.

Available from:

NASA Center for AeroSpace Information (CASI)
7121 Standard Drive
Hanover, MD 21076-1320
(301) 621-0390

National Technical Information Service (NTIS)
5285 Port Royal Road
Springfield, VA 22161-2171
(703) 605-6000

Abstract

We demonstrate instantaneous flow density visualization of the boundary layer region of a Mach 2.5 supersonic flow over a flat plate that is interacting with an impinging shock wave. Tests were performed in the Unitary Plan Wind Tunnel (UPWT) at NASA Langley Research Center. The technique is elastic light scattering using 10-nsec laser pulses at 532 nm. We emphasize that no seed material of any kind, including water (H_2O), is purposely added to the flow. The scattered light comes from a residual impurity that normally exists in the flow medium after the air drying process. Thus, the technique described here differs from the traditional vapor-screen method, which is typically accomplished by the addition of extra H_2O vapor to the airflow. The flow is visualized with a series of thin two-dimensional light sheets (oriented perpendicular to the streamwise direction) that are located at several positions downstream of the leading edge of the model. This geometry allows the direct observation of the unsteady flow structure in the spanwise dimension of the model and the indirect observation of the boundary layer growth in the streamwise dimension.

Introduction

Langley Research Center's (LaRC) Unitary Plan Wind Tunnel[1] (UPWT) is one of three nearly identical supersonic flow facilities in the U.S. that has been heavily used in the development of supersonic aircraft and missiles since the 1950's. In addition to schlieren, the only other standard method for off-body flow visualization in these tunnels is vapor-screen[2–4] visualization, sometimes referred to as laser light sheet visualization. In this method, water (H_2O) is injected into the facility to increase the light scattering cross section of the flow medium. An Argon-ion laser beam is then swept through the flow near the model by using a scanning mirror to direct the beam into the tunnel test section. The scattered light that visualizes flow structures is then recorded on videotape for later data analysis. These images are acquired at the standard video rate (i.e., integrated over 1/30-sec); thus, short-lived supersonic flow structures will be washed out when imaged over this relatively long 1/30-sec window. Also, it is well-known that large amounts of H_2O in the flow medium can significantly modify the flow parameters. For example, the increased drag on a model or the increased pressure reading of a pitot tube are two typical[5] indications used to detect strong condensation effects in transonic wind tunnels. Additionally, free-stream stagnation conditions are known[3,6] to be altered up to ~10% after the condensation of large amounts of H_2O in the UPWT. Flow visualization without H_2O addition can minimize these problems.

In this report, we discuss flow visualization at the UPWT by using elastic light scattering off the dry flow medium with high-intensity, short-pulse lasers. This type of flow imaging complements the capabilities of the currently used methods of schlieren and vapor screen. The elastic light scattering method is truly noninvasive (i.e., no probes or excessive H_2O in the flow and no optical excitation of the flow medium). In addition, this technique can capture high-speed temporal structure and image it with good spatial resolution. With Nd:YAG lasers (Neodymium : Yittrium Aluminum Garnet, i. e., $Nd^{3+} : Y_3 Al_5 O_{12}$), the flow can be imaged in 10^{-8} sec, which effectively freezes the flow down to scales of 0.01 mm. Most flow visualization reported before ~1990 involved visualizing the scattered light from some type of seed material (i.e., not a component of typical air), where the question arises of "how well does the seed material disperse and follow the airflow?" At the molecular level, Rayleigh scattering does not suffer from this potential problem.

Laser-based elastic light scattering for two-dimensional flow visualization of low-speed fluids consisting of heavy molecules was demonstrated[7,8] about 15 years ago by using visible wavelengths. This technique was extended[9] to supersonic airflow by using the relatively larger scattering cross section at ultraviolet (UV) wavelengths. More recently, this method has been tested[10] in large-scale flow facilities and subsequently used for experimental studies[11] of the dynamics of fuel-oxidizer mixing at Mach 6. Another attraction of elastic light scattering, in the absence of cooling-induced condensation[12–15] of the flow constituents, is that currently available high-power lasers are intense enough to illuminate the flow at the molecular level without seeding any foreign material into the flow. This situation allows for quantitative off-body flow field density measurements[16,17] with high spatial resolution in two dimensions. Many laboratory-type demonstrations of elastic light scattering have been made over the last five years. For example, density, temperature, and velocity imaging[17–19] in one and two spatial dimensions has been demonstrated.

Even with the relatively weak scattering at the visible wavelength of 532 nm, scattered light levels are strong enough to visualize the flow (without seeding) at Mach 2.5 inside the UPWT at NASA LaRC. We conjecture that a normally occurring low-level impurity in the flow of this particular wind tunnel has a large scattering cross section compared to molecular air. We are able to visualize the flow without the injection of H_2O into the wind tunnel because the light scatter by this impurity is strong. The scattering signals are strong enough to visualize flow features with a single 10-nsec laser pulse, so these data represent instantaneous images with the flow frozen in time. We present 2-dimensional images of a flat plate boundary layer flow that is perturbed with an impinging shock wave. This work extends previous laboratory work on boundary layer visualization to a large-scale facility that is often used by the aeronautical industry.

The shock wave/boundary layer interaction model that we study in this work was originally designed and built for another project (unpublished work by Ira J. Walker, Lockheed Engineering and Sciences, 1993). We originally worked with this model to obtain nonintrusive off-body stimulated Raman data for comparison to surface pressures. During the course of the Raman work on this model, we noticed some anomalous intensity noise on one of the Raman laser beams. We postulated that this extra intensity noise might be due to beam steering from turbulent, unstable, or unsteady flow near the model. To help analyze the Raman data, we decided to use some tunnel time to obtain Rayleigh images of the boundary layer. However, the Rayleigh images provide useful flow visualization; thus, we present them in this report.

To illustrate the widespread potential of this type of flow visualization, we also discuss one-dimensional flow visualization in the supersonic vortices above a delta wing. This vortex-related work was performed prior to the shock wave/boundary layer work and in the same wind tunnel at Mach 2.8. It was this unanticipated vortex visualization that prompted us to try the boundary layer visualization.

Experimental Setup

Unitary Plan Wind Tunnel

Figure 1 shows a schematic of the experimental configuration used for the shock wave/boundary layer interaction model. We use a Q-switched Nd:YAG laser that is frequency doubled to wavelength $\lambda = 532$ nm and that delivers 120 mJ per laser pulse (10 pulses/sec) into the test section of the wind tunnel. By using a 91-cm focal length cylindrical lens, the beam is focused into a thin, vertical light sheet that is 1 cm high. The thickness of this sheet along the free-stream flow direction is about 200 μm and is approximately constant over the 38-cm width of the model. The viewing angle θ is 30 deg, and the laser beam is linearly polarized in the free-stream direction. The detector is a Princeton Applied Research

intensified-charge-coupled device (ICCD) camera that images the laser beam region with either an f/4.5 Nikon or a 75 mm Fujinon zoom lens.

All images shown in this report were acquired with the bottom edge of the laser sheet positioned about 1.2 cm above the lower surface of the model. Thus, we are probing the boundary layer region from 1.2 to 2.2 cm above the lower plate surface at five streamwise locations. This height was as close as we could put the laser beam to the surface without generating significant scatter from the surface because we made only a quick attempt to aperture the beam as it transited from the laser to the wind tunnel. This lack of effort was dictated by the short time available to execute this work. With longer planning and setup time, we would be able to better reduce the scattered light and get the beam significantly closer to the surface, if required for thinner boundary layers. However, for the flow and model combination studied here, 1–2 cm from the surface is close enough to observe the boundary layer height that varies from near zero at the leading edge to about 2–3 cm at some downstream locations.

This work was performed in the 1.2 by 1.2-meter test section 2 at the UPWT of LaRC. The free-stream flow conditions are Mach 2.5 and unit Reynolds number 6.5×10^6 per meter. For these tests, the flow medium is dry air. A schematic of the shock wave/boundary layer interaction model is shown in figure 1. Figure 2a shows the model mounted in the test section, while figure 2b shows the view that we see from our camera, with the Fujinon zoom lens adjusted for a relatively wide field of view. The dark protrusions in the bright light sheet illustrate the unsteady edge of the boundary layer, where low-density boundary layer fluid mixes into the denser free-stream fluid. In figure 2b, the laser beam is located 7.6 cm downstream of the shock impingement point. Replacing the Fujinon lens with the Nikon f/4.5 lens allows us to see an image, under higher magnification, of one half of the field of view of figure 2b. Figure 3 shows an example of the light sheet with the higher magnification. The schematic of figure 4 shows the five locations on the model where light-sheet data were acquired. For our 2.5-cm-diameter lenses, the solid angle of collection is about 5×10^{-4} sr.

Laboratory Calibration

We reproduced our wind tunnel setup in the laboratory after the tunnel tests were completed to calibrate the absolute strength of the scattered signals from the UPWT. In the laboratory setup, we used the same beam geometry, laser powers, and signal collection geometry as in the facility. We used small sample pieces of the schlieren quality windows from the UPWT to reproduce beam intensity reductions due to reflections. A low-speed flow of bottled Nitrogen (N_2) at the exit of an 8-cm diameter pipe was used to create a dust-free sample region. Using this setup, we measured the magnitude of the molecular Rayleigh scattering at 1 atm and 300 K on our camera. Since the two setups are so similar, these laboratory data are used to estimate the strength of the UPWT facility signals relative to the molecular air signals in the laboratory.

Results and Discussion

Laboratory Calibration

Comparing the laboratory signals from dust-free N_2 to the signals from the UPWT facility, we conclude that the free-stream flow from the facility produces a scattered light level that is about 500 times larger than what is expected from Rayleigh scattering from pure N_2 or air. Inspection of the images obtained in the free stream (see fig. 5a) shows that the scattered light level is uniform on all scales that we can resolve (from the width of the model to the limit of our resolution, about 300–500 μm) with the Nikon lens. Therefore, the scattered light signals that we detect are likely from a normally occurring

impurity that is uniformly distributed throughout the airflow. We are **definitely not** directly detecting the N_2 and oxygen (O_2) molecules of the airflow.

Nature of the Scattering Species

Scatterers whose size is much less than the light wavelength λ produce Rayleigh scattering, while scatterers whose size is much greater than λ produce Mie Scattering. These two types of scattering have different magnitudes and angular dependencies.

If the flow constituent responsible for the scattered signal is not from air molecules, we need to determine what it is, how uniformly it is mixed with the air, and how well it follows the supersonic flow. Oil is known to be in the flow (e.g., oil accumulates on the test section windows after running the tunnel at high Reynolds number [1.3×10^7 per meter] for long periods of time). Several possible impurities are (1) dust or dirt particles; (2) small clusters, or large droplets of condensed oil; (3) clusters or ice crystals of residual H_2O; and (4) clusters of argon (Ar), carbon dioxide (CO_2), N_2 or O_2 molecules. The arguments, detailed below, concerning the nature of the scattering centers and our conclusions based on these arguments are summarized in table 1. The possibilities are listed in order of increasing probability for contributing to the observed signal, as determined by our subjective decision based on the comments in the right-side column. Because of the relatively large static temperature of 150 K and relatively small static pressure of 0.05 atm in the test section free-stream flow, we strongly believe that it is unlikely that the air molecules (except CO_2) are clustering or condensing significantly. The temperature of 150 K is well above the boiling point for N_2, O_2, and Ar for a pressure of 0.05 atm.

Using some qualitative observations of the data images, we can eliminate some of the possible sources of scatter that are listed above. If one ignores the expected variation due to the nonuniform

Table 1. Summary of Potential Scattering Species in LaRC's UPWT, Along With Qualitative Estimates for Occurrence of Each Species

Possible scatterer	Chance of occurrence	Comment
N_2 clusters	Low	Not likely at 150 K and 0.05 atm
O_2 clusters	Low	Not likely at 150 K and 0.05 atm
Ar clusters	Low	Not likely at 150 K and 0.05 atm
Mixed molecule clusters	Low	Literature does not contain much discussion on mixed species clusters.
Dust or dirt	Medium	a) Data clearly shows dia. $\leq$ 200 mm. b) Data also suggests dia. $\leq$ 86 nm. c) UPWT contains no filters; very small (<10 μm) dust is possible.
CO_2 clusters	Medium	We estimate 3000 CO_2-CO_2 collisions in one nozzle transit.
H_2O clusters	Medium	We estimate 3000 H_2O-H_2O collisions in one nozzle transit (i.e., $[H_2O] \approx [CO_2]$ for dew point = 244 K).
Oil clusters	High	Oil condenses on windows for long runs at large Reynolds numbers.

beam profile, the images that are obtained in the free-stream flow show uniform light scattering over large regions of flow. The very bright scatter from room air dust that typically saturates many adjacent detector pixels is almost completely absent when the tunnel is running. We also note that the large signal from typical dust at atmospheric pressure in the test section (with no flow) is about 30 times larger than the impurity signal that we detect at Mach 2.5 flow conditions. Large particle scatterers cannot produce the relatively small and uniform signals that we see in the free-stream flow data. Thus, we do not put large ($>> \lambda$) dirt, dust, or oil particles high on our list of likely scatterers, but we cannot rule out very small ($\leq \lambda$) sizes of these species.

Using some details of the collection geometry, we can estimate[10] the minimum density of the scatterers. We assume that there must be at least one scatterer or more per volume element that is imaged onto each camera pixel because the free-stream images are so uniform. The camera pixels are 11.5×25 μm in size and the magnification of our collection lens is 1/16. Since the laser sheet is about 200 μm thick, we estimate that each camera pixel images 3×10^{-5} cm^3. The reciprocal of this number, 3.3×10^4 cm^{-3}, is the minimum number density that the scattering species must have to obtain one imaged scatterer per camera pixel and produce the uniform signal that is observed.

Next, we can use this minimum number density to estimate the maximum size of the scatterers. Recall that the free-stream signals are about 500 times that of dust-free room air and that the size of room air molecules is about 0.1 nm. Assuming that the scattering process is Rayleigh, rather than Mie, the scattering cross section is proportional to the particle diameter to the 6th power, thus allowing one to write the equality,

$$[500]\, N_r\, [0.1\ \text{nm}]^6 = N_i\, [D]^6,$$

where N_r is the room air molecular density, N_i is the wind tunnel impurity number density, and D is the maximum possible size of the impurities in units of nm. Thus, we obtain D = 86 nm for the maximum size of the free-stream impurity scatterers.

Since the laser light wavelength λ is 532 nm, we cautiously conclude from this maximum size that the scattering process is in the Rayleigh ($\lambda >> D$) regime. However, note that we had to assume that the process was Rayleigh to use the fact that the signal is proportional to the 6th power of the particle diameter. Mie scattering ($\lambda << D$) signals will vary much less than the 6th power of diameter. Thus, the argument of the last paragraph is somewhat circular, and we lose some confidence in the conclusion that the scattering process is Rayleigh. We cannot definitively rule out Mie scattering from particles ($\approx$ few μm in diameter), where several of these particles could potentially fit in the sample volume of each camera pixel to yield the uniform images that we observe.

Residual Water

The typical dew point of the flow is about 244 K, depending on the outside weather. With this small amount of H_2O in the flow and the 10-m length of the expansion nozzle, we roughly estimate only 3000 H_2O-H_2O collisions during the expansion. Assuming that clustering occurs under these conditions, that every collision sticks (i.e., 3000 molecules per cluster), and that there is 10^{-7} Torr vapor pressure of H_2O at 150 K, we then estimate an H_2O cluster density of 2×10^6 cm^{-3}. This density is two orders of magnitude larger than the previous estimate for the minimum scatterer density. Thus the estimated H_2O cluster density is consistent with our observation of uniform scattering on our smallest resolved spatial dimensions, as calculated in the preceding two paragraphs. We cannot use this calculation to rule out H_2O as the scatterer. However, we present a last argument that implies that H_2O condensation is unlikely to contribute to our signals.

The following argument contains three unproven assumptions and should be taken as our opinion of the most reasonable scenario, but not necessarily as rigorous fact. Consider that the scatterer is not H_2O. Assume that the scatterer is mixed such that it makes up a constant mole fraction of the flow density. We compare the brighter (larger density) free-stream signals to the dimmer (smaller density) boundary layer signals. For most of the data, the bright regions of the free stream are measured to be about 2.7 ±0.6 times brighter than the dark regions of boundary layer material that is mixing upward. This measurement is the average of 15 ratio measurements made from 15 different individual video frames. The uncertainty of ±0.6 is the statistical (1 σ = 68% confidence) error for the sample of 15 ratios. The 15 different frames were chosen from light sheet locations 2–5 of figure 4 and there is no obvious trend in the measured ratio with location. Stray background light from window scatter and the ICCD dark current are approximately accounted for in each individual frame by measuring the signal levels in pixels just below the edge of the laser beam and subtracting this level from the total signal level in the laser beam regions of interest. This approximate method for subtracting stray light and dark current backgrounds is used since it is not possible (due to leaks) to evacuate the UPWT test section to a density that is much lower than the static density during the run, which would allow a more accurate background subtraction on a pixel by pixel basis.

It is useful to compare this measurement with the expected density ratio. Assuming isentropic expansion throughout the nozzle, we can calculate the free-stream density. If we assume constant pressure and that the boundary layer regions are frictionally heated back to the stagnation temperature (temperature recovery = 1), then we also know the boundary layer density. The calculated ratio of free-stream to boundary layer density is the ratio of the stagnation temperature to the free-stream temperature or about 325 K/150 K = 2.2, in agreement with the measurement of 2.7 ±0.6. Thus the observed signals are proportional to the two densities (free-stream and boundary layer) that we know with some degree of confidence. This result is consistent with the assumption that the impurity that is responsible for the scattered signal is uniformly mixed and follows the flow reasonably well. For example, if the flow density changes by a factor of two, then we expect that the impurity density and the scattering signal will also change by a factor of two.

On the other hand, consider that the scatterer is condensed H_2O that is partially or completely evaporated in the hot boundary layer and undergoes increased clustering when cooled to the free-stream temperatures. Although not impossible, it is a remarkable coincidence if the increase in signal is also a factor of two — due to an increase of the clustering rate of the cool free-stream relative to the warm boundary layer. Thus, we also believe, although less confidently than for the other possibilities, that it is unlikely that H_2O is clustering or condensing just enough to provide the observed scattering signal that seems to be proportional to density.

Determination of the Scattering Species

Based on these arguments, we believe that the strongest candidate for our signal source is small clusters of oil in the flow. Unfortunately, we can not specify with absolute confidence what is contributing to our scattered light signal. The somewhat speculative nature of some of the previous arguments is less than satisfactory, and more work is necessary to identify the scatterer unambiguously.

In the next three sections, we shall assume that a uniform (i.e., constant mole fraction) oil impurity in the flow consists of small clusters that accurately follow the flow and make the only contribution to our scattered light signal. Thus, the signal is proportional to the total flow density. Hence, regions of bright signal indicate higher airflow densities and dimmer signals indicate smaller airflow densities. In figures 2b, 3, and 5, the small, cloud-like dark regions that protrude upwards into the narrow bright band of the laser light sheet are eruptions of hot (~325 K) boundary layer material. These hotter regions are

just starting to mix upward into the colder (~150 K) and denser free-stream flow that is more brightly illuminated by the laser light sheet. If we are wrong, and the scattering species is H_2O, for example, it will not significantly change any of the discussion of the flow visualization that follows.

Visualization of Shock/Boundary Layer Region

We have visualized the flow in two-dimensional sheets perpendicular to the streamwise direction, concentrating on the boundary region (i.e., 1–2 cm above the surface) between the free-stream flow and the boundary layer. We initially used the Fujinon zoom lens to obtain relatively wide fields of view. An example is the image of figure 2b, which shows a segment of the laser light sheet that is about 30 cm long. We have also imaged narrower fields of view by using the f/4.5 Nikon lens, where the imaged region is shown in figure 3.

All images presented in this report do not have the stray background contributions subtracted. However, the signal-to-background ratio is sufficiently large to display clear flow structure.

One example of a raw data image is shown in figure 3a, which shows a magnified view from the central region of the model that is centered on the centerline of the model. The width of this field of view is about 15 cm, i.e., less than half of the 38 cm-width of the model. Figure 3b shows the same data after the contrast has been enhanced for display purposes. This is the same field of view that is displayed in figure 5. The purpose of figure 3 is to convince the reader that we have not unreasonably altered the raw images with our image enhancement process. Details of the image enhancement of the original 8-bit images are as follows. Linear contrast stretching and image smoothing are both used. The linear contrast stretching technique involved choosing two gray levels (here 20 and 100) in the original image and linearly mapping each gray level value within this specified range onto the entire gray level range of 0 to 255. All gray level values that fall below and above the specified range are clipped to zero (black) or 255 (white), respectively. The image-smoothing technique reduces high-frequency noise by replacing the gray level at each pixel with the average of the gray levels in a 3 by 3 neighborhood.

To sequentially probe different locations, we have qualitatively visualized the growth of the turbulent boundary layer thickness as a function of distance downstream from the leading edge of the model by translating the model in the streamwise direction. A two-dimensional composite of the model and five laser light sheet locations are shown in figure 4. The five locations are (1) 5 cm upstream of the leading edge, i.e., the free stream; (2) 16 cm downstream of the leading edge, i.e., about 1/2 the streamwise distance down the shock-generating ramp; (3) 22 cm downstream of the leading edge, i.e., the shock impingement point; (4) 5.1 cm farther downstream of the impingement point; and (5) 7.6 cm downstream from the impingement point.

Figures 5a–e show eight successive single-shot images obtained for each of the five different streamwise locations that are shown in figure 4 and described in the preceding paragraph. In other words, figure 5a shows eight sequential images from position 1, the free-stream location of figure 4; figure 5b shows eight sequential images from position 2, 1/2 way down the ramp and so forth. Each individual image of figure 5 is a 10-nsec shot of flow field and hence gives an instantaneous picture of the upper boundary layer structure. At each location, the eight different images were acquired at a 10-Hz repetition rate. The data at each location were typically acquired about 2–5 minutes after the preceding upstream location. All images of figure 5 are enhanced in the same manner as figure 3b.

The net result of figure 5 is to show both the instantaneous flow structure that is transverse to the streamwise direction in each image and the growth or decay of the boundary layer with streamwise location over the entire set of images. Location 2 is the furthest upstream position where we are able to

see the first hints of transverse structure at this height off the surface. All positions upstream of this location give images that show a uniform light sheet and are indistinguishable from images at the free-stream location; we interpret this to mean that the boundary layer thickness in smaller than 1.2 cm, which is the distance from the lower edge of the laser sheet to the lower surface of the model. Hence, we have not illustrated any locations between the leading edge and location 2 in figures 4 and 5.

At location 2 and farther downstream, we see the roughly bimodal structure that is shown throughout figures 5b–e. By bimodal, we mean that the bright regions of the laser sheets usually display about twice the signal level as the darker cloud-like structures that protrude up into the bottom of the sheet. We interpret these darker regions as hot boundary layer gas mixing upward into the brighter regions of colder free-stream flow. The images of figure 5 vividly illustrate the spanwise inhomogeneity of the boundary layer on an instantaneous timescale. Moving downstream, the maximum height of these structures occurs near location 3, the shock impingement point. Farther downstream at locations 4 and 5, the maximum height of these regions decreases, as shown in the figure.

Thus, we observe a boundary layer thickness that increases with increasing downstream distance from the leading edge and reaches a maximum height at the position (i.e., location 3 in fig. 4) where the shock impinges on the lower plate. Downstream from this location, the boundary layer thickness begins to decrease, with farther increasing distance downstream. This variable boundary layer height is consistent with typical descriptions[20–22] of shock/boundary-layer flow fields, where the boundary layer separates from the surface near the shock impingement point and reattaches farther downstream. This behavior is also in agreement with schlieren data obtained on this model. At the impingement point, schlieren data show a maximum boundary layer thickness of about 2 cm, consistent with the maximum height (~2.2 cm or larger) of the flow structures in figure 5.

The centers of the light sheets of the figure 5 images correspond to the center of the model. Inspection of all figure 5 images shows that the hot boundary layer protrusions into the cold free-stream flow seem to occur more often on the left-hand side of the laser sheet than on the right-hand side. Note that attenuation of the laser beam, as it transits the test section, is negligible and thus does not play a role in this observation. This observation is confirmed by reviewing about 10,000 total images (spanning 2–3 hours of run time) that were acquired during the entire test. At any location that shows the mixing structures, we always see a thicker boundary layer, on the average, on the right-hand side, as compared to the left-hand side. We believe that, for whatever reason, this observation suggests that the boundary layer is growing asymmetrically over the bottom plate for these particular setup and run conditions, thus illustrating a spanwise inhomogeneity of the boundary layer in a time-integrated sense. This kind of observation is not possible with the standard schlieren data because schlieren signals are averaged over a line of sight.

Note that the shock structure was too weak to detect with this particular combination of laser intensity, wavelength, and viewing angle.

One-Dimensional Visualization

During the stimulated Raman experiments that immediately preceded this flow visualization work, we had visualized this same boundary layer region with the laser beam focused to a narrow line that crossed the model at the same locations as the sheets shown in figure 4. Thus, we imaged narrow lines of flow field that are perpendicular to the streamwise direction and parallel to the bottom plate. The laser energy/pulse was about 40–50 mJ, and the 532 nm light was focused to minimum diameter of about 200 μm at the centerline of the model. The line of laser light was placed 8 mm above the surface

of the lower plate. The scatter by the flow medium was large enough that the line of laser light could be seen with the naked eye in the near forward and backward directions.

The results of this one-dimensional variation of flow visualization are in qualitative agreement with the results of the sheet imaging described previously and are illustrated with reproductions of hand sketches (that we made while observing, by naked eye, the beam in real time) in figure 6. The data were recorded in this manner only because we were in the middle of Raman experiments and not able to acquire images with the ICCD camera. Three streamwise locations are shown in figure 6, corresponding to positions 1, 3, and 4 of figure 5. In the free stream, the beam brightness was uniform in both time and the spanwise direction. At shock impingement point 3, the beam became completely invisible inside the model boundaries but remained steadily bright outside the model boundaries. Farther downstream at position 4, the beam appeared intermittent in both time and the spanwise dimension inside the model, but remained steadily bright outside the model.

These results are consistent with both the schlieren and sheet-imaging results described previously. At the impingement point, the low-density boundary layer has grown thick enough (and has also separated from the surface) to completely overlap the beam and reduce the scattered signal from regions inside the model. At downstream position 4, the boundary layer has decreased just enough that some of the largest hot regions of boundary layer material protrude up into the beam to create several dark spots in the beam across the width of the model. The spatial intermittence of the laser beam rapidly varies with time, illustrating the high-speed temporal dependence of the boundary layer height as a function of spanwise location. This temporal behavior is washed out in most conventional space-averaged or time-averaged schlieren images.

Delta Wing Vortex Visualization

To illustrate the general applicability of this technique, we briefly describe the results of flow visualization of the vortices above a delta wing in a Mach 2.8 supersonic flow. This work was done in the UPWT prior to the boundary layer visualization. The angle of attack is 12 deg. The energy/pulse is 40 mJ. In the delta wing work, the 532-nm laser beam is not focused into a sheet but is again focused into a line (perpendicular to the model centerline) with a 120-cm focal length spherical lens. Thus only line images perpendicular to the free-stream direction can be visualized.

The geometry is shown in figure 7, where the free-stream flow is out of the plane of the paper in the end view depictions of figures 7a and 7b, and is from left to right in the side view depiction of figure 7c. The line of the focused laser beam is perpendicular to the free-stream flow, and the flow was visualized by naked eye observation in the near forward direction, as illustrated in figure 7a. The results were recorded with hand sketches and are shown in figure 7. In the free-stream flow, i. e., upstream of the model, the laser beam appeared as a uniform and steadily bright line where the beam crossed the tunnel test section (as shown in fig. 7a). The model was translated along the direction of the flow until the beam was located about 6 mm above the delta wing, as shown in the side view of figure 7c. Primary and secondary vortices were clearly observed as abrupt "dark holes" in the laser beam, as shown in figure 7b. We emphasize that this visualization was done without any seeding or purposeful increase in the normal amount of H_2O (dew point = 244 K) in the flow.

This flow visualization was performed during the same time frame as that used for the acquisition of both nonintrusive Raman data and five-hole-probe velocity data (unpublished work, James E. Byrd, Lockheed Martin, 1993). The probe was mounted such that it could be translated, along the streamwise direction, from far downstream of the trailing edge of the model to the position just upstream of the trailing edge that contained the laser beam. The probe was used as a reference marker for the placement

of the crossing position of the Raman beams by locating the crossing inside of the vortex at a known probe position. On one day of Raman data acquisition, we backed the probe far downstream of the model after positioning the Raman beams. On a second day, the probe tip was left just upstream of the trailing edge after positioning the Raman beams. We believe that we observed a significant difference in the transverse position of the vortex between these two longitudinal probe positions. Two problems (i.e., the limited tunnel time and the naked eye detection with the awkward geometry of observing along a line in the near forward direction of the laser beam) hindered this observation. The less-than-ideal nature of this observation leaves us uncertain of the tentative conclusion that the presence of the probe near the trailing edge moves the position of the vortex. However, this observation at supersonic velocities is consistent with a similar report[23] of a seven-hole-probe that influenced the position of a vortex at subsonic speeds.

Summary

We have demonstrated the visualization of the boundary layer regions of an inlet model in the normal unmodified test gas of a Mach 2.5 free-stream flow in NASA-Langley's UPWT facility. Flow visualization has been performed previously with schlieren or by seeding large amounts of extra H_2O into the flow. We have shown that one can use 532 nm to visualize the supersonic flow in a large-scale facility because of the relatively high light scattering cross section of an impurity contained in the dry air flow. With the caveat that the impurity is uniformly mixed and follows the flow, the signal is proportional to total density, and the images presented here are representative of the total flow density. Although the nature of the impurities that provide our scattering signal are not known with complete confidence at this time, there is evidence that suggests that the size of these impurities is less than 86 nm. We believe that the two most likely possibilities for the light scatterers that we observe are oil or residual H_2O.

Our geometry allows us to observe the nonuniform flow structure in the dimension transverse to the free-stream flow direction. We also observe the growth of the boundary layer height due to an impinging shock wave. This work illustrates the potential of future laser-based, instantaneous, nonintrusive flow visualization of boundary layer regions in this (or a similar) facility. In future work, a geometry orthogonal to the one used in this work would allow the instantaneous flow visualization of the boundary layer, including transition from laminar to turbulent flow, in a streamwise direction on an instantaneous timescale. Quantitative measurements, if possible in the UPWT, will require more detailed work of calibrating the raw data in the wind tunnel itself and account for stray light backgrounds and other possible systematic errors. We have also demonstrated the visualization of the vortices generated by supersonic flow over a delta wing using the same technique as used in the boundary layer work.

For future work, we suggest tests to investigate the nature of the scattering signal that we are observing in the UPWT facility. Precise knowledge of the scattering species would give more confidence in any aerodynamic conclusions that are drawn from work based on the noninvasive flow visualization technique described in this report.

References

1. C. M. Jackson, Jr., W. A. Corlett, and W. J. Monta, "Description and Calibration of the Langley Unitary Plan Wind Tunnel," NASA TP-1905 (November 1981).

2. W. L. Snow and O. A. Morris, "Investigation of Light Source and Scattering Medium Related to Vapor-Screen Flow Visualization," NASA TM-86290 (December 1984).

3. O. A. Morris, W. A. Corlett, D. L. Wassum, and C. D. Babb, "Vapor-Screen Technique for Flow Visualization in the Langley Unitary Plan Wind Tunnel," NASA TM-86384 (July 1985).

4. I. McGregor, "The Vapour-Screen Method of Flow Visualization," J. Fluid Mech. **11**, 481–511 (1961).

5. R. M. Hall, "Studies of Condensation Effects on Airfoil Testing in the Langley 0.3-Meter Transonic Cryogenic Tunnel." NASA TP-2509 (January 1986).

6. P. P. Wegener and L. M. Mack, "Condensation in Supersonic and Hypersonic Wind Tunnels," in *Advances in Applied Mathematics*, Vol. 5, edited by H. L. Dryden and Th. von Kármán, Academic Press, NY, pp. 307–447 (1958).

7. M. C. Escoda and M. B. Long, "Rayleigh Scattering Measurements of the Gas Concentration in Turbulent Fields," AIAA J. **21**, 81–84 (1983).

8. B. Yip, D. C. Fourguette, and M. B. Long, "Three-Dimensional Gas Concentrations and Gradient Measurements in a Photoacoustically Perturbed Jet," Appl. Opt. **25**, 3919–3923 (1986).

9. M. Smith, A. Smits, and R. Miles, "Compressible Boundary-Layer Density Cross Sections by UV Rayleigh Scattering," Opt. Lett. **14**, 916–918 (1989).

10. B. Shirinzadeh, M. E. Hillard, and R. J. Exton, "Condensation Effects on Rayleigh Scattering Measurements in a Supersonic Wind Tunnel," AIAA J. **29**, 242–246 (1991).

11. B. Shirinzadeh, M. E. Hillard, R. J. Balla, I. A. Waitz, J. B. Anders, and R. J. Exton, "Planar Rayleigh Scattering Results in Helium-Air Mixing Experiments in a Mach-6 Wind Tunnel," Appl. Opt. **31**, 6529–6534 (1992).

12. J. V. Becker, "Results of Recent Hypersonic and Unsteady flow Research at the Langley Aeronautical Laboratory," J. Appl. Phys. **21**, 619–628 (1950).

13. P. P. Wegener, "Nucleation of Nitrogen: Experiment and Theory," J. Phys. Chem. **91**, 2479–2481 (1987).

14. P. P. Wegener, Chapter 4, in *Nonequilibrium Flows*, Part 1, edited by P. P. Wegener, Marcel Dekker, Inc, NY, pp. 163–243 (1969).

15. B. Shirinzadeh, M. E. Hillard, A. B. Blair, and R. J. Exton, "Study of Cluster Formation and its Effects on Rayleigh and Raman Scattering Measurements in a Mach 6 Wind Tunnel," AIAA paper # 91-1496, 22nd Fluid Dynamics, Plasma Dynamics, & Lasers Conference, Honolulu, HI (24–26 June 1991).

16. B. Shirinzadeh, R. J. Balla, and M. E. Hillard, "Quantitative Density Measurements in a Mach 6 Flow Field Using the Rayleigh Scattering Technique," 1995 ICIASF, Wright-Patterson AFB, OH (18–21 July 1995).

17. R. G. Seasholtz, "Instantaneous 2D Velocity and Temperature Measurements in High Speed Flows Based on Spectrally Resolved Rayleigh Scattering," AIAA paper # 95-0300, 33th Aerospace Sciences Meeting, Reno, NV (1995).

18. R. B. Miles, J. N. Forkey, and W. R. Lempert, "Filtered Rayleigh Scattering Measurements in Supersonic/ Hypersonic Facilities," AIAA paper # 92-3894, 17th Aerospace Ground Testing Conference, Nashville, TN (6–8 July, 1992).

19. G. Grünefeld, V. Beushausen, and P. Andresen, "Planar Air Density Measurements Near Model Surfaces by Ultraviolet Rayleigh/Raman Scattering," AIAA J. **32**, 1457–1463 (1994).

20. U. Domröse, E. Krause, and M. Meinke, "Numerical Simulation of Laminar Hypersonic Shock-Boundary Layer Interaction," Z. Flugwiss. Weltraumforsch. **20**, 89–94 (1996).

21. F. S. Alvi and G. S. Settles, "Physical Model of the Swept Shock Wave/Boundary-Layer Interaction Field," AIAA Journal **30**, 2252–2258 (1992).

22. Henckels, A. F. Kreins, and F. Maurer, "Experimental Investigation of Hypersonic Shock-Boundary Layer Interaction," Z. Flugwiss Weltraumforsch **17**, 116–124 (1993).

23. J. T. Kegelman and F. W. Roos, "The Flowfields of Bursting Vortices Over Moderately Swept Delta Wings," AIAA-90-0599, 28th Aerospace Sciences Meeting, Reno, NV (1990).

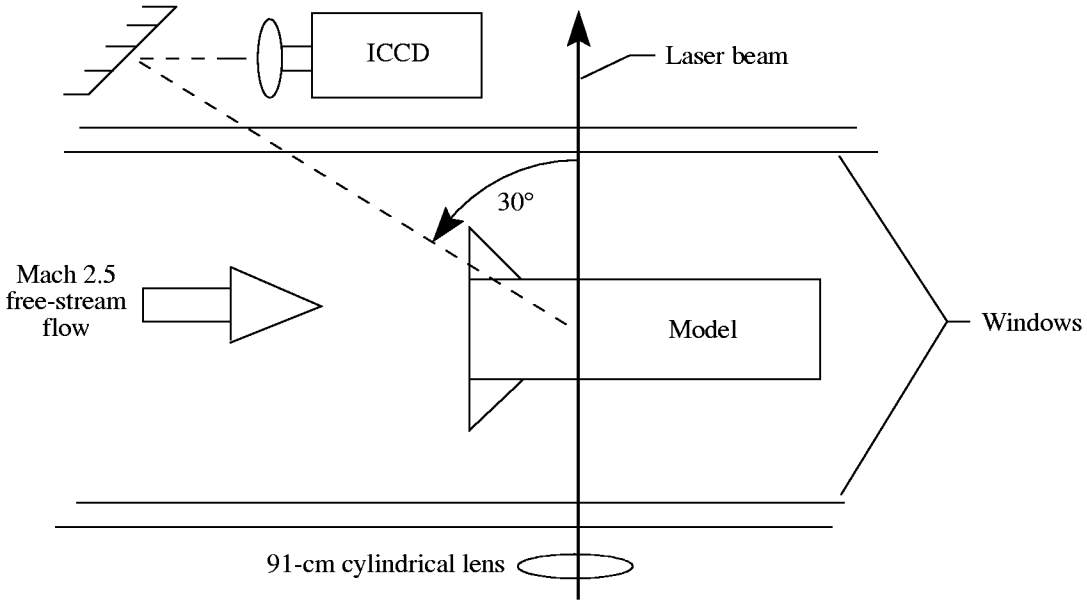

(a) Top view.

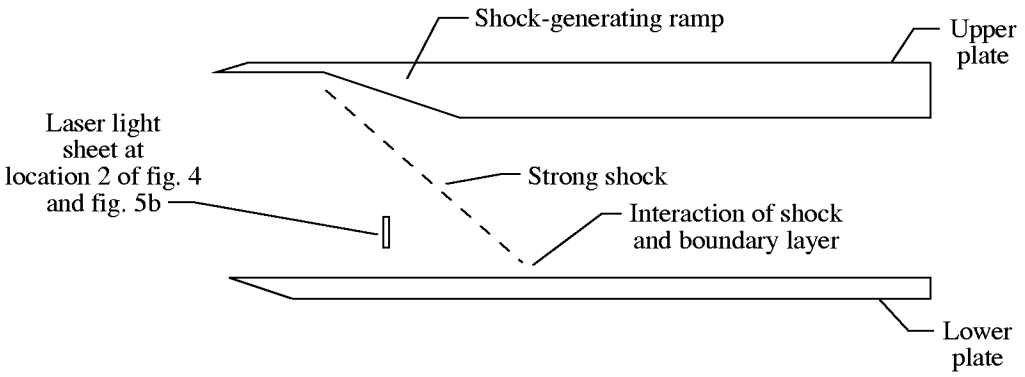

(b) Side view.

Figure 1. Diagram of experimental arrangement for flow visualization of flat plate boundary layer region showing views from the top and side. The laser beam, collection optics, and camera are fixed relative to the wind tunnel test section. Different longitudinal positions along the model are viewed by translating the model inside the test section along the free-stream flow direction. (Figure not to scale.)

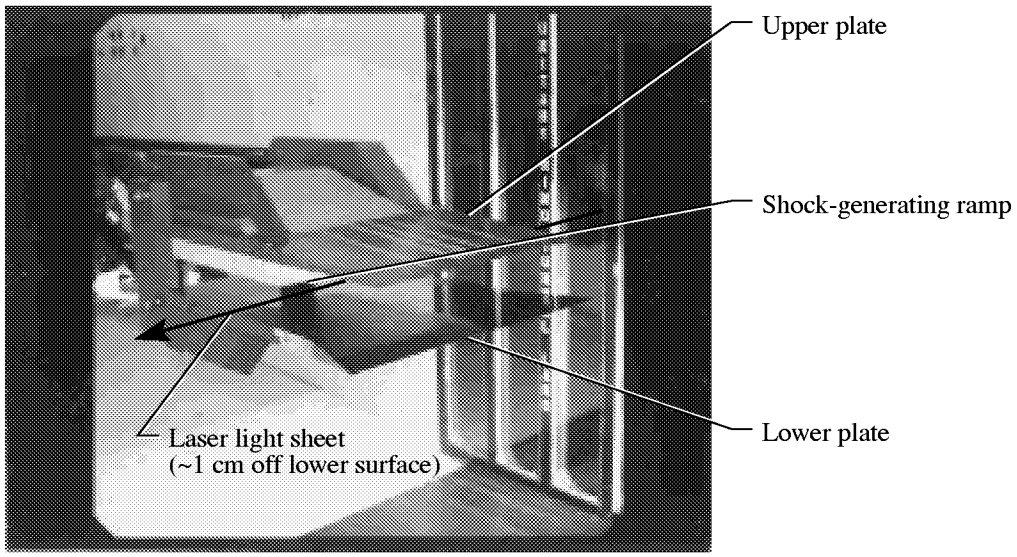

(a) Photograph of shock boundary layer interaction model in UPWT test section.

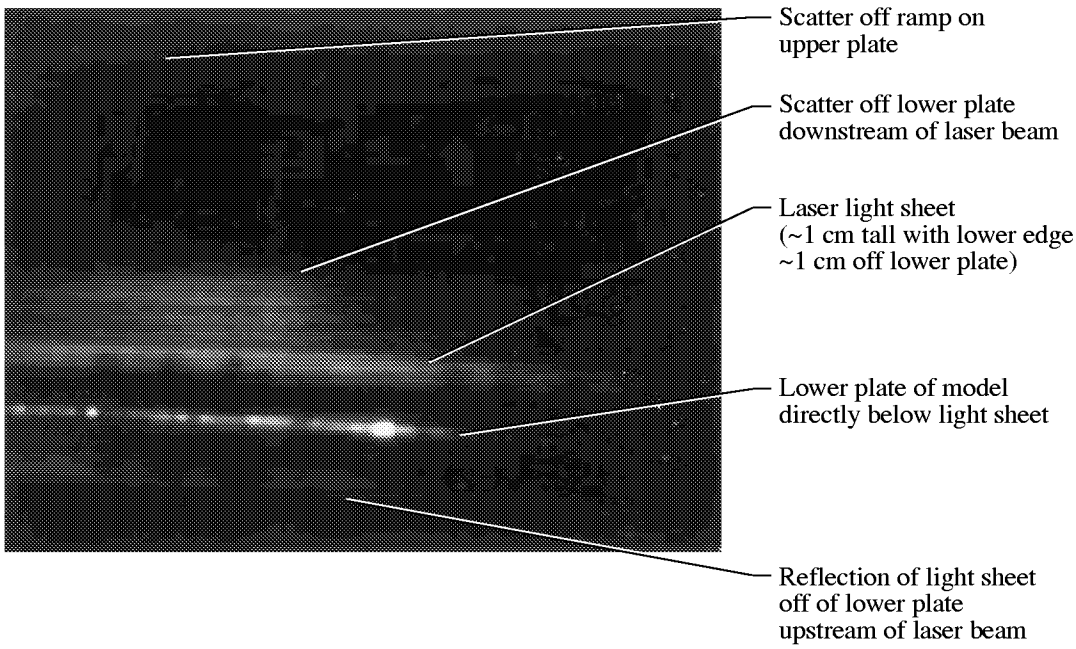

(b) ICCD image of boundary layer region.

Figure 2. Shock-boundary layer interaction model in the UPWT test section and ICCD image of the boundary layer region (illuminated by laser light), using a wide field of view.

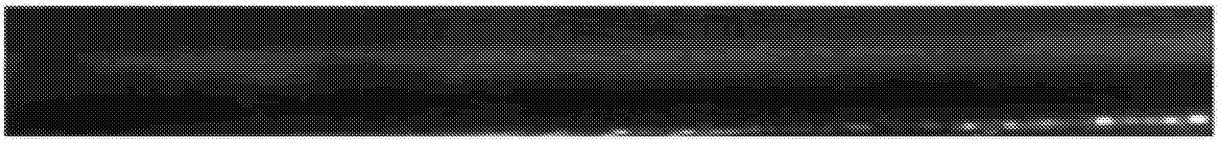

(a) Raw image.

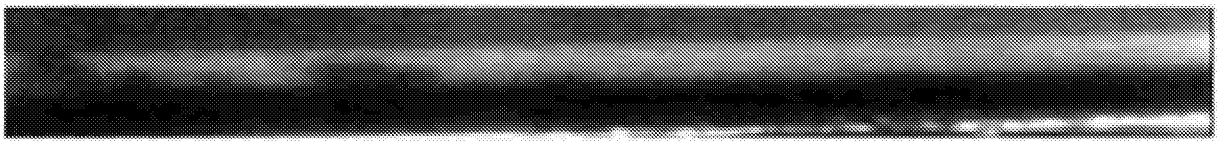

(b) Contrast-enhanced version.

Figure 3. The raw and contrast-enhanced version of same image.

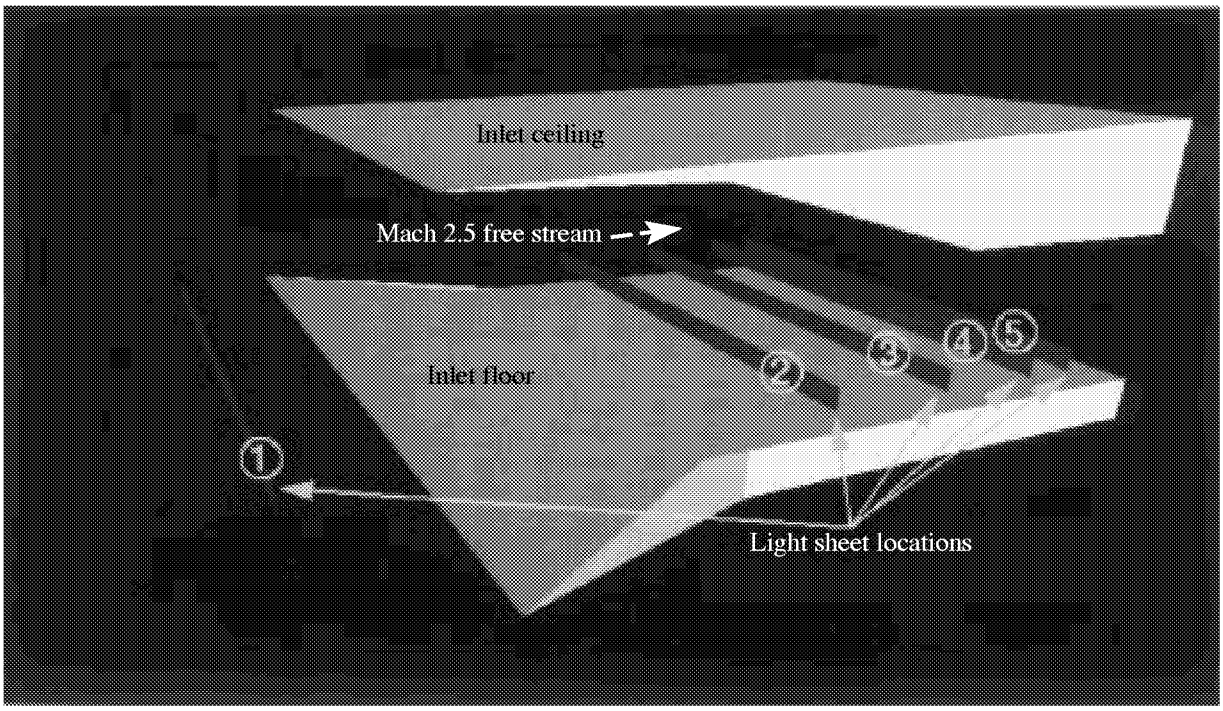

Figure 4. Illustration of model and five laser light sheets, with each sheet shown at a different streamwise position. The five locations are (1) 5 cm upstream of leading edge (i.e., the free stream); (2) 16 cm downstream of the leading edge (i.e., about 1/2 way down the shock-generating ramp on the upper plate); (3) 22 cm downstream (i.e., the shock impingement point); (4) 5.1 cm farther downstream of impingement point; and (5) 7.6 cm downstream from impingement point. Single pulse images (for each of five locations) are shown in figure 5.

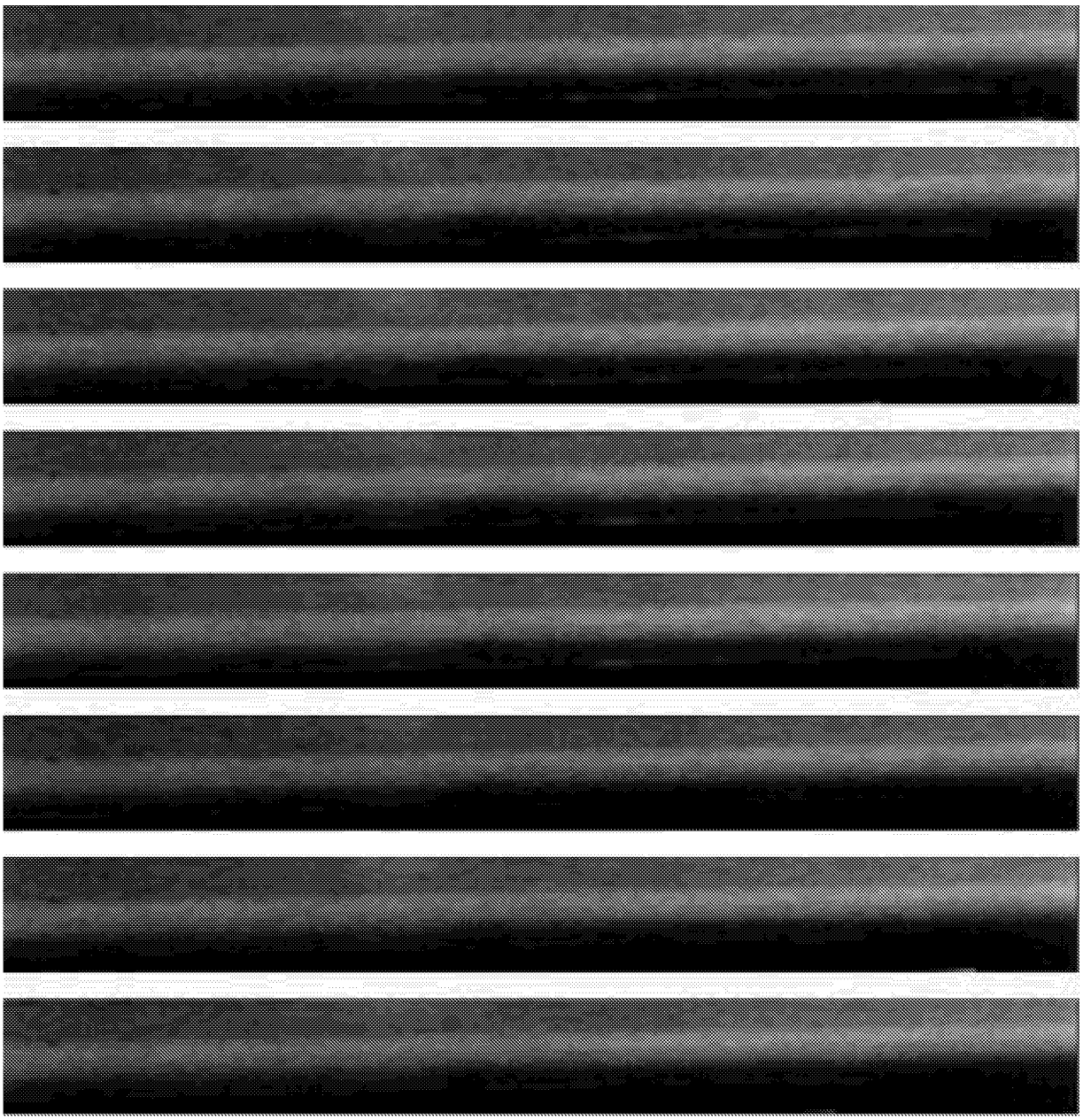

(a) Location 1.

Figure 5. Successive single pulse (i.e., instantaneous) sheets of flow structure as a function of distance downstream from leading edge of model. Locations 1 through 5, described in figure 4, respectively correspond to parts (a) through (e) of this figure. All images are with the same magnification as in figure 3. For each location we show eight successive laser shots at 0.1 sec temporal separation.

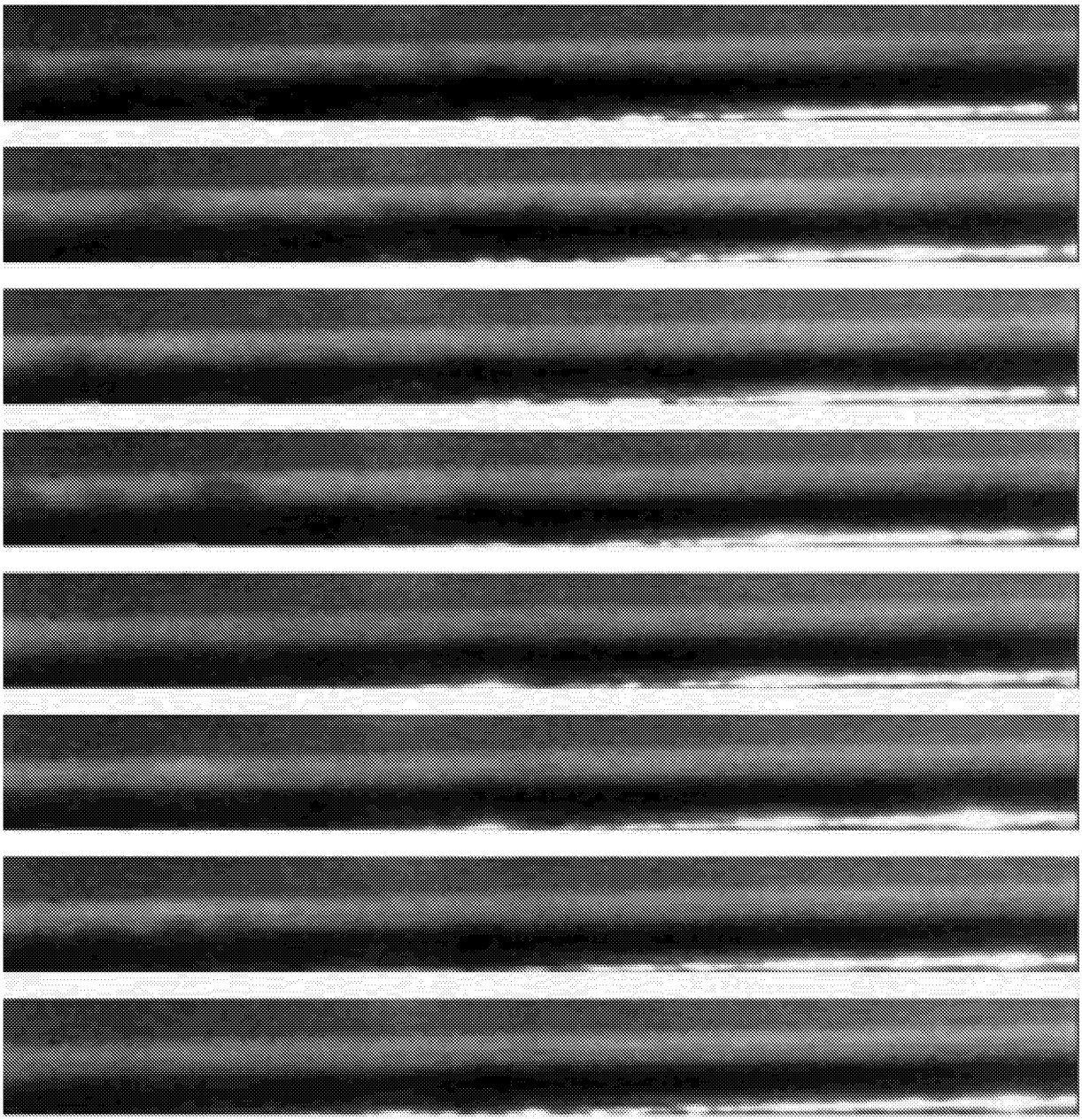

(b) Location 2.

Figure 5. Continued.

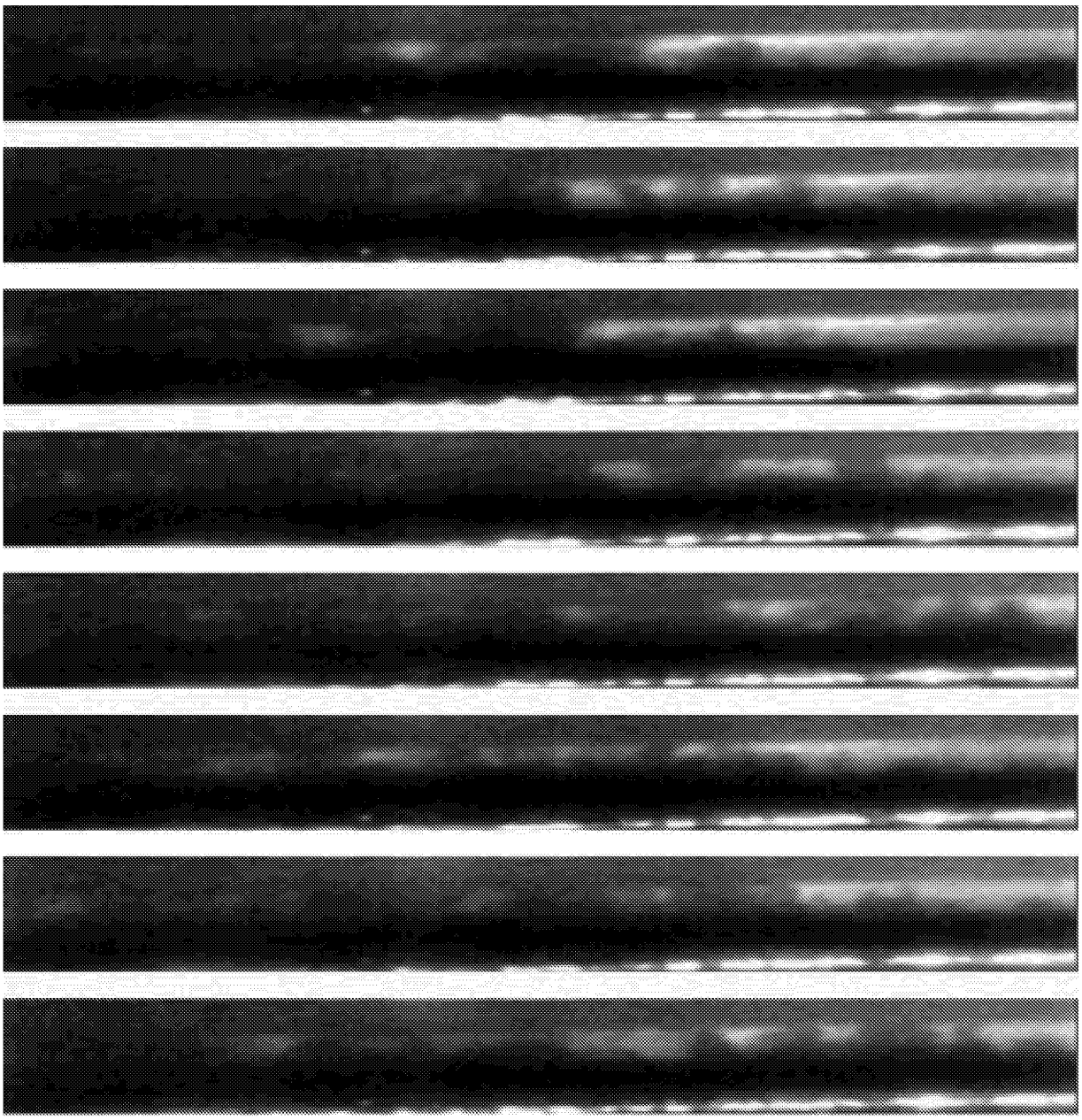

(c) Location 3.

Figure 5. Continued.

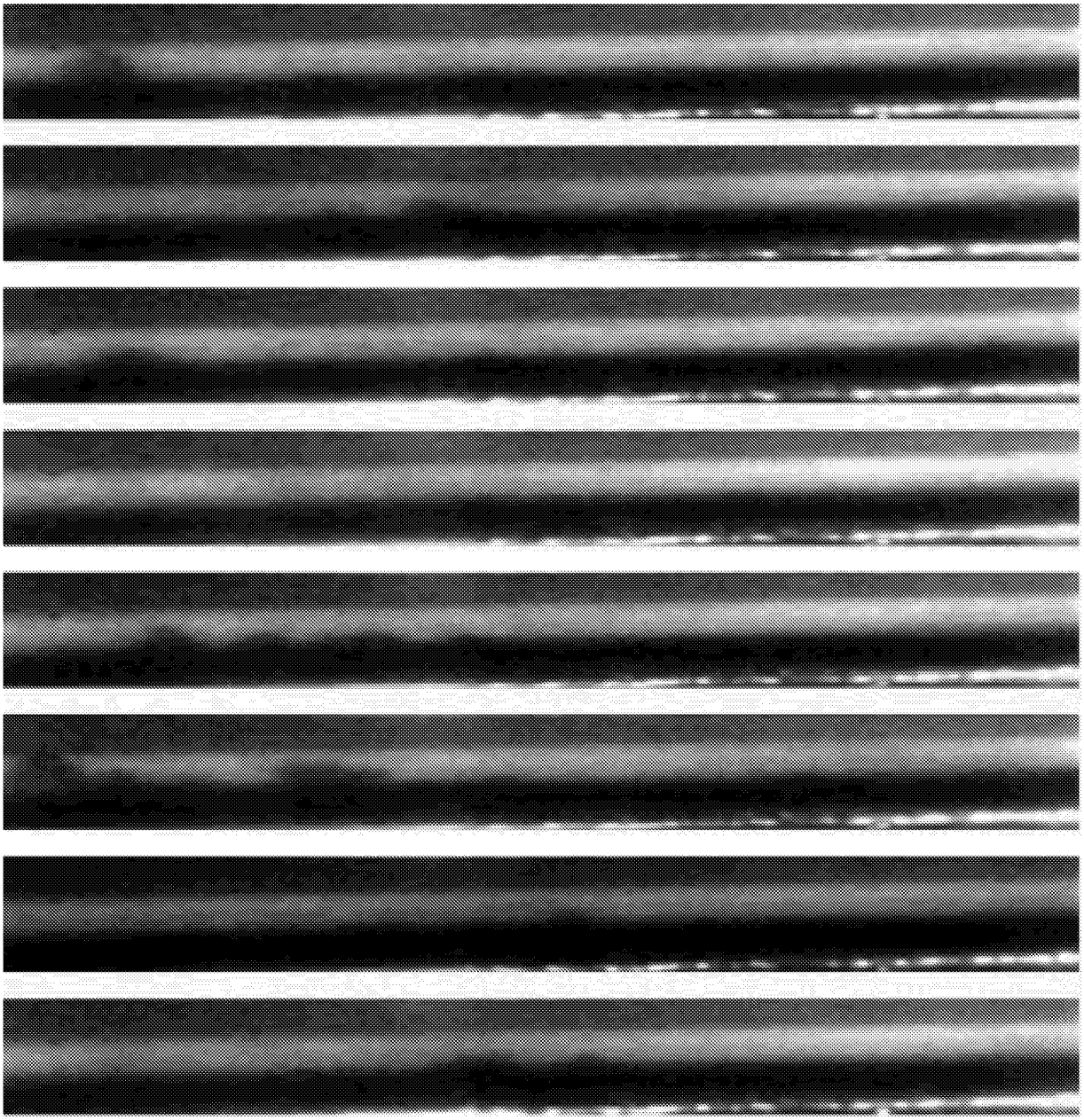

(d) Location 4.

Figure 5. Continued.

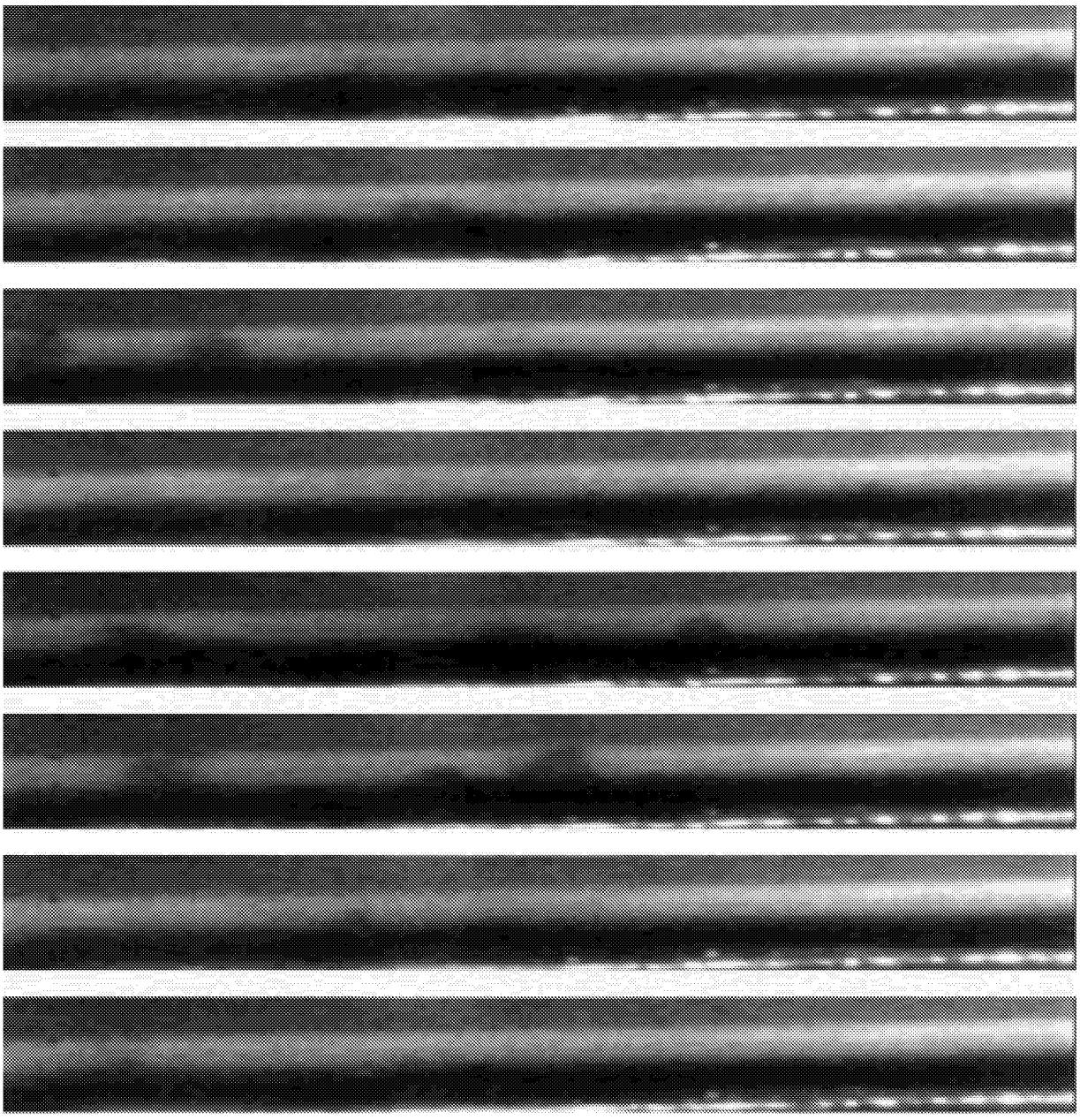

(e) Location 5.

Figure 5. Concluded.

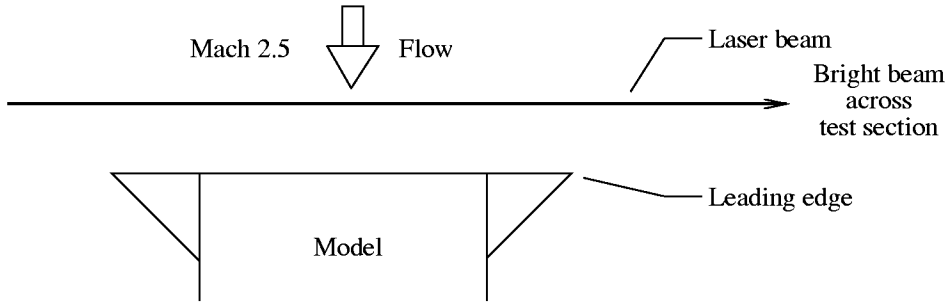

(a) Free-stream position. (Location 1)

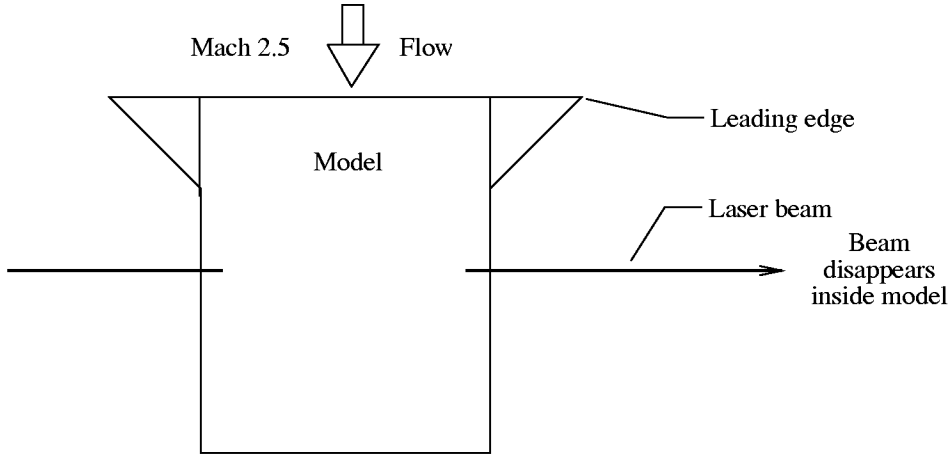

(b) Impingement point position. (Location 3)

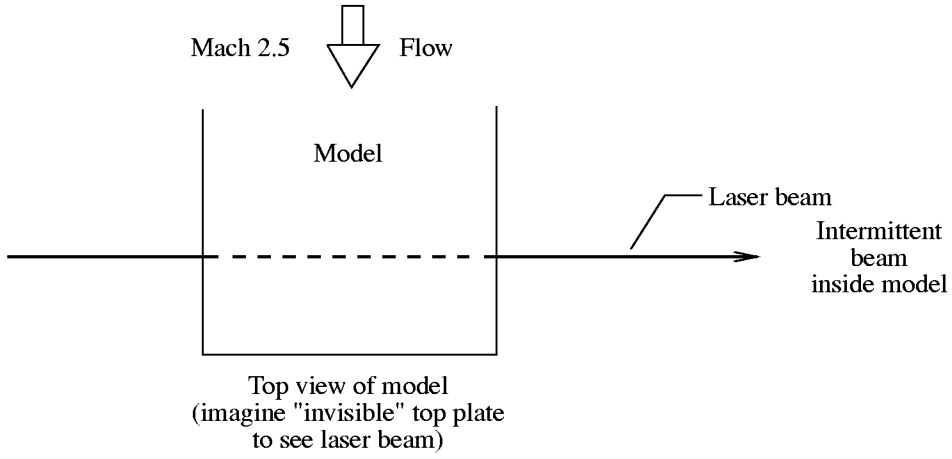

(c) Position 7.6 cm downstream of impingement point. (Location 5)

Figure 6. Sketch of line imaging made from visual observations of boundary layer region from a shock-boundary layer interaction model. Three illustrated positions (free stream, impingement point, and 7.6 cm downstream of impingement point) correspond to (a), (c), and (e) of figure 5. The narrow focused beam is 8 mm above model surface.

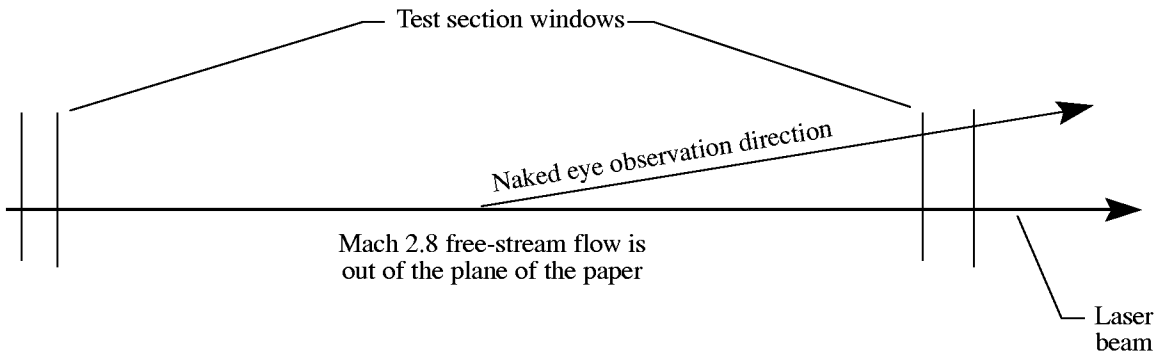

(a) Uniform intensity of beam in free stream.

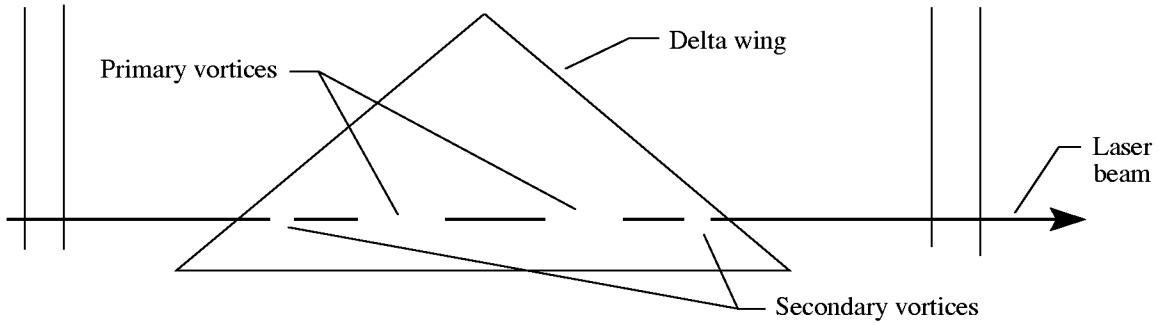

(b) Primary and secondary vortices.

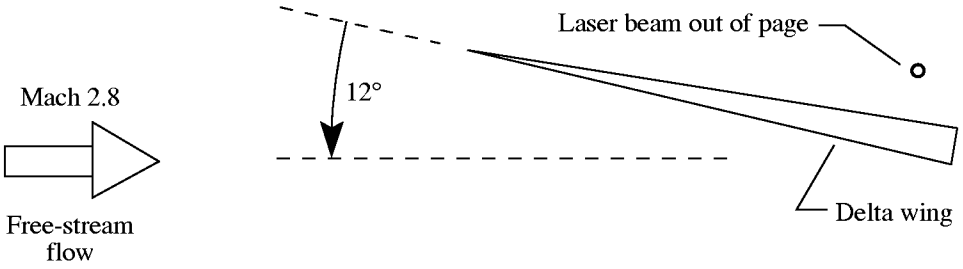

(c) Side view.

Figure 7. Sketch of line imaging made from visual observations of the supersonic flow field of the vortices above a delta wing. The uniform intensity of beam in the free stream is illustrated in (a), while the four gaps in the beam show low density regions of the two primary and two secondary vortices in (b). The side view of (c) shows the approximate location of the beam relative to the wing.

REPORT DOCUMENTATION PAGE

Form Approved
OMB No. 0704-0188

1. AGENCY USE ONLY *(Leave blank)*	2. REPORT DATE	3. REPORT TYPE AND DATES COVERED
	August 2000	Technical Memorandum

4. TITLE AND SUBTITLE
Flow Visualization by Elastic Light Scattering in the Boundary Layer of a Supersonic Flow

5. FUNDING NUMBERS
WU 522-31-61-01

6. AUTHOR(S)
G. C. Herring and Mervin E. Hillard, Jr.

7. PERFORMING ORGANIZATION NAME(S) AND ADDRESS(ES)
NASA Langley Research Center
Hampton, VA 23681-2199

8. PERFORMING ORGANIZATION REPORT NUMBER
L-17960

9. SPONSORING/MONITORING AGENCY NAME(S) AND ADDRESS(ES)
National Aeronautics and Space Administration
Washington, DC 20546-0001

10. SPONSORING/MONITORING AGENCY REPORT NUMBER
NASA/TM-2000-210121

11. SUPPLEMENTARY NOTES

12a. DISTRIBUTION/AVAILABILITY STATEMENT
Unclassified–Unlimited
Subject Category 74 Distribution: Standard
Availability: NASA CASI (301) 621-0390

12b. DISTRIBUTION CODE

13. ABSTRACT ***(Maximum 200 words)***

We demonstrate instantaneous flow visualization of the boundary layer region of a Mach 2.5 supersonic flow over a flat plate that is interacting with an impinging shock wave. Tests were performed in the Unitary Plan Wind Tunnel (UPWT) at NASA Langley Research Center. The technique is elastic light scattering using 10-nsec laser pulses at 532 nm. We emphasize that no seed material of any kind, including water (H_2O), is purposely added to the flow. The scattered light comes from a residual impurity that normally exists in the flow medium after the air drying process. Thus, the technique described here differs from the traditional vapor-screen method, which is typically accomplished by the addition of extra H_2O vapor to the airflow. The flow is visualized with a series of thin two-dimensional light sheets (oriented perpendicular to the streamwise direction) that are located at several positions downstream of the leading edge of the model. This geometry allows the direct observation of the unsteady flow structure in the spanwise dimension of the model and also allows the indirect observation of the boundary layer growth in the streamwise dimension.

14. SUBJECT TERMS	15. NUMBER OF PAGES
Rayleigh scattering; Boundary layers; Supersonic flow	28
	16. PRICE CODE: A03

17. SECURITY CLASSIFICATION OF REPORT	18. SECURITY CLASSIFICATION OF THIS PAGE	19. SECURITY CLASSIFICATION OF ABSTRACT	20. LIMITATION OF ABSTRACT
Unclassified	Unclassified	Unclassified	UL